Beam Update Rate Analysis for Low-Complexity Hybrid Beamforming in LEO Satellites

Mohammad Momani, Thomas Delamotte and Andreas Knopp
Institute of Information Technology, University of the Bundeswehr Munich, 85579 Neubiberg, Germany
Email: paper.sp@unibw.de, {firstname.lastname}@unibw.de

***Abstract*—Massive antenna arrays with hybrid beamforming offer enhanced antenna gain and beam steering flexibility for low Earth orbit (LEO) satellite communications, balancing flexibility, complexity and power consumption. However, efficient beamforming implementation is challenging due to satellites' high velocity, limited power and computational constraints. In this paper, we investigate the update rate requirements of the analog and digital beamforming coefficients for various LEO altitudes and antenna array sizes, using a low-complexity discrete Fourier transform (DFT) codebook for analog beam steering and zero-forcing (ZF) digital precoding to minimize inter-beam interference. Simulation results show that analog beam steering updates are generally manageable—requiring realignment in the range of seconds—even for lower orbits and larger arrays. In contrast, digital precoding updates are more stringent, requiring updates in the order of tens of milliseconds to prevent a significant decline in performance. Moreover, we demonstrate the need to optimize analog beam steering codebooks to adapt to the satellite's service area. Finally, we propose a digital precoding update algorithm to optimize the trade-off between update rate and system performance.**

***Index Terms*—DFT codebook, hybrid beamforming, low-complexity satellites, non-terrestrial networks (NTN), phased antenna arrays.**

I. Introduction

Non-terrestrial networks (NTNs) have emerged as a promising solution to address the limitations of terrestrial networks (TNs), which, although globally deployed in populated areas, often struggle to provide reliable connectivity in remote regions like deserts, oceans, and mountains. These underserved areas present significant challenges for conventional TNs. NTNs have the potential to bridge this connectivity gap, offering global coverage, especially in such remote areas, making them essential components of future communication systems. Furthermore, NTNs are anticipated to play a critical role in disaster relief by ensuring communication continuity when TN infrastructure is compromised or absent [1].

Satellite constellations are categorized by orbital altitude, which influences key performance characteristics, including velocity, coverage area and latency. The three primary categories are geostationary Earth orbit (GEO), medium Earth orbit (MEO), and low Earth orbit (LEO) satellites, which are the main focus in this work.

In LEO satellite systems, two main approaches are employed for coverage: Earth-moving beams and Earth-fixed beams [2]. Earth-moving beams have fixed beam directions relative to the satellite, causing the coverage area to move across the Earth's surface as the satellite orbits. This movement necessitates that users in a specific ground area switch to different beams over time to maintain continuous coverage. Conversely, Earth-fixed beams create stationary coverage areas on the ground by dynamically steering the spot beams to maintain alignment with specific locations. The key distinction is whether the coverage area moves with the satellite or stays fixed on the ground [3].

The beam steering mechanism employed in satellites with Earth-fixed beams is crucial for achieving precise beam pointing, ensuring that link budget requirements are met. Digital beam steering is particularly advantageous for LEO satellites due to its high pointing precision, which is essential for closing the link budget and reducing inter-user interference [4]. However, fully digital beamforming requires a dedicated RF chain for each antenna element, resulting in high hardware complexity and low energy efficiency, especially in large-scale multiple-input and multiple-output (MIMO) systems [5]. In such systems, large antenna arrays generate a high number of beams for optimal coverage, further exacerbating these issues. Given LEO satellites' limited power and size, this is impractical. In contrast, fully analog beamforming requires a single RF chain, allowing only one data stream to be transmitted at any given time. Additionally, fully analog beamforming makes it difficult to implement advanced beamforming techniques, such as nulling in specific directions, because it lacks the flexibility of digital signal processing. Hybrid beamforming offers a compromise between these two extremes by enabling simultaneous multi-stream communications while significantly reducing the number of RF chains needed compared to the total number of antenna elements [6].

In large-scale MIMO systems, where beams must cover a wide range of angles, analog beam steering codebooks are adopted to overcome hardware limitations and improve channel estimation and feedback efficiency. These codebooks consist of a predefined set of beams, with each beam covering a specific direction, collectively spanning the entire space. One example of a codebook is the discrete Fourier transform (DFT) codebook [7]. In LEO satellite communications, codebooks are particularly useful for optimizing the beamforming process, especially in scenarios involving massive MIMO antenna systems. These codebooks are effective for beamforming with arrays of various shapes and sizes, including large-scale two-dimensional uniform planar arrays [8].

This research was funded by dtec.bw – the Digitalization and Technology Research Center of the Bundeswehr – which is financed by the European Union under the NextGenerationEU initiative.

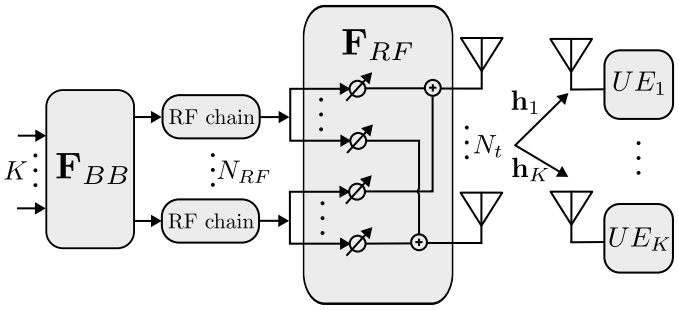

Fig. 1: System Model.

A review of the literature reveals a gap in understanding the analog and digital beamforming coefficients update requirements for the highly mobile LEO satellites, particularly when beams must maintain optimal alignment with fixed ground locations. Accordingly, this study aims to analyze the required time for beamforming coefficient updates in a hybrid beamforming system, with a particular focus on the continuity of service for ground users. The rest of the paper is organized as follows: Section II describes the system model and basic assumptions. Section III describes the proposed hybrid beamforming strategy. Section IV outlines the simulation parameters, the required analog beam update rate across varying orbital heights and antenna array sizes, and discusses the digital precoding update requirements for mitigating inter-user interference and its impact on the system sum-rate.

Notation: $\mathbf{a}$ is a vector and $\mathbf{A}$ is a matrix. The operators $|.|$, $(.)^H$, $(.)^T$, $(.)^\dagger$ and $||.||_F$ denote the absolute value, conjugate transpose, transpose, Moore–Penrose pseudo inverse and Frobenius norm, respectively. The Kronecker product of vectors $\mathbf{a}$ and $\mathbf{b}$ is denoted as $\mathbf{a} \otimes \mathbf{b}$. The identity matrix is denoted as $\mathbf{I}$.

II. System and Channel Model

The satellite is equipped with $N_t = N_x \times N_y$ antenna elements arranged in a fully-connected hybrid beamforming architecture, with N_x and N_y being the number of antenna elements in the x and y directions, respectively. The satellite is communicating with K single-antenna user equipment (UEs) and the number of RF chains at the satellite satisfies $N_{RF} \geq K$ assuming that each UE receives a single data stream and $N_{RF} \ll N_t$. The system model is illustrated in Fig. 1.

Given that LEO satellite channels are typically line-of-sight (LOS) dominant [9], the single-path LOS channel between the satellite and the k^{th} UE is expressed as

$$\mathbf{h}_k = \alpha_k \, \widetilde{\mathbf{h}}_k, \tag{1}$$

where, α_k represents the k^{th} UE LOS gain parameter, incorporating the distance-dependent free-space path loss and atmospheric losses and $\widetilde{\mathbf{h}}_k = \sqrt{N_t}\, \mathbf{a}^H(\theta_k, \phi_k)$. The satellite's 3D array manifold vector $\mathbf{a}(\theta_k, \phi_k) \in \mathbb{C}^{N_t \times 1}$ is given as

$$\mathbf{a}(\theta_k, \phi_k) = \frac{1}{\sqrt{N_t}} \left[e^{j\boldsymbol{\kappa}^T \mathbf{r}_0}, e^{j\boldsymbol{\kappa}^T \boldsymbol{r}_1}, \ldots, e^{j\boldsymbol{\kappa}^T \boldsymbol{r}_{N_t}} \right]^T, \tag{2}$$

where (θ_k, ϕ_k) are the downlink azimuth and elevation angles of departure of the k^{th} UE, $\boldsymbol{\kappa} = \frac{2\pi}{\lambda} [\sin\theta_k \cos\phi_k, \sin\theta_k \sin\phi_k, \cos\theta_k]^T$ is the plane wave wavenumber, λ is the wavelength and $\mathbf{r}_n = [x_n, y_n, z_n]^T$ is the position column vector of the n^{th} satellite antenna element.

Let $\mathbf{x} = [x_1, x_2, \ldots, x_K]^T \in \mathbb{C}^{K \times 1}$ be the transmitted symbol vector for K users, satisfying $\mathbb{E}\{\mathbf{x}\mathbf{x}^H\} = \mathbf{I}_K$, then the received signal at the k^{th} UE can be written as

$$y_k = \mathbf{h}_k \, \mathbf{F}_{RF} \, \mathbf{F}_{BB} \, \mathbf{x} + z_k, \tag{3}$$

where, $\mathbf{F}_{RF} \in \mathbb{C}^{N_t \times N_{RF}} = [\mathbf{f}_{RF,1}, \mathbf{f}_{RF,2}, \ldots, \mathbf{f}_{RF,N_{RF}}]$ is the analog beamforming matrix, with each vector satisfying the constant modulus constraint, i.e., $||\mathbf{f}_{RF,n}||^2 = 1$ for $n = 1, \ldots, N_{RF}$, $\mathbf{F}_{BB} \in \mathbb{C}^{N_{RF} \times K} = [\mathbf{f}_{BB,1}, \mathbf{f}_{BB,2}, \ldots, \mathbf{f}_{BB,K}]$ is the digital precoding matrix and $z_k \sim \mathbb{C}\mathcal{N}(0, \sigma_z^2)$ is the additive white Gaussian noise (AWGN) with zero mean and variance $\sigma_z^2 = k_B T B$, where k_B, T and B are the Boltzman constant, noise temperature and bandwidth, respectively.

Let P_t be the satellite's total transmit power, with equal power allocated to each UE, then the system sum-rate can be formulated as

$$R_{sum} = \sum_{k=1}^{K} \log_2 \left(1 + \frac{\frac{P_t}{K} \left| \mathbf{h}_k \, \mathbf{F}_{RF} \, \mathbf{f}_{BB,k} \right|^2}{\frac{P_t}{K} \sum_{i \neq k} \left| \mathbf{h}_k \, \mathbf{F}_{RF} \, \mathbf{f}_{BB,i} \right|^2 + \sigma_z^2} \right). \tag{4}$$

III. Proposed Beamforming Strategy

Our hybrid beamforming scheme is designed to achieve two primary objectives: first, to maximize the signal-to-noise ratio (SNR) in the analog domain for each individual UE k, and second, to reduce the inter-beam interference using digital processing. Similar to [10], the problem of designing $\mathbf{F}_{RF}$ and $\mathbf{F}_{BB}$ can be decoupled in two independent stages.

A. Analog Beam Steering

For the k^{th} UE, the satellite selects an analog beam from a predefined set of beams derived from a DFT codebook, with the objective of maximizing the signal-to-noise ratio (SNR) while disregarding the interference from other UEs. This can be formulated as follows

$$\begin{aligned} \mathbf{f}_{RF,k}^{opt} = & \arg\max_{\mathbf{f}_{RF,k}} \left| \mathbf{h}_k \, \mathbf{f}_{RF,k} \right|^2 \\ & \text{subject to } \mathbf{f}_{RF,k} \in \mathcal{U}, \, \forall \, k, \\ & \qquad ||\mathbf{f}_{RF,k}||^2 = 1, \forall k, \end{aligned} \tag{5}$$

where, $\mathcal{U} \in \mathbb{C}^{N_t \times O N_t}$ is the 2D DFT analog beam steering codebook with oversampling factor $O \in \mathbb{R}_{>0} = O_x O_y$, with O_x and O_y being the oversampling factor along the x and y directions, respectively. The 2D codevectors are given as

$$\mathbf{u}^{(m,l)} = \mathbf{u}_x^{(m)} \otimes \mathbf{u}_y^{(l)}, \tag{6}$$

for $m = 0, 1, \ldots, O_x N_x - 1$ and $l = 0, 1, \ldots, O_y N_y - 1$. $\mathbf{u}_x^{(m)}$ and $\mathbf{u}_y^{(l)}$ are the 1D DFT codebooks along the x and y directions, respectively, and are written as

$$\begin{aligned} \mathbf{u}_x^{(m)} &= \frac{1}{\sqrt{N_x}} \left[1,\, e^{\frac{j2\pi}{O_x N_x} m},\, \ldots,\, e^{\frac{j2\pi}{O_x N_x}(N_x-1)m}\right]^T, \\ \mathbf{u}_y^{(l)} &= \frac{1}{\sqrt{N_y}} \left[1,\, e^{\frac{j2\pi}{O_y N_y} l},\, \ldots,\, e^{\frac{j2\pi}{O_y N_y}(N_y-1)l}\right]^T. \end{aligned} \tag{7}$$

For the analog beam switching strategy, the satellite continuously monitors the SNR of each UE and performs an analog beam switch when a new beam offers a higher SNR than the current one.

B. Digital Precoding Interference Mitigation

Once the analog beamforming matrix, $\mathbf{F}_{RF}$, has been determined from (5), the equivalent channel, $\hat{\mathbf{h}}_k$ for the k^{th} UE can be expressed as

$$\hat{\mathbf{h}}_k = \widetilde{\mathbf{h}}_k \, \mathbf{F}_{RF}, \tag{8}$$

which depends on the positions of the UEs, which needs to be acquired at least once for UEs that are stationary or quasi-stationary, eliminating the need for continuous feedback. The multi-user equivalent channel, $\hat{\mathbf{H}}$, can be constructed as

$$\hat{\mathbf{H}} = \left[\hat{\mathbf{h}}_1^T,\, \hat{\mathbf{h}}_2^T,\, \ldots,\, \hat{\mathbf{h}}_K^T\right]^T. \tag{9}$$

To minimize the inter-user interference, we adopt zero-forcing (ZF) digital precoding, which can be computed by taking the pseudo inverse of the equivalent channel as

$$\mathbf{F}_{BB} = \hat{\mathbf{H}}^{\dagger}. \tag{10}$$

Additionally, the digital precoding matrix $\mathbf{F}_{BB}$ is normalized to satisfy the total transmit power limit such that

$$||\mathbf{F}_{RF}\, \mathbf{F}_{BB}||_F^2 = K. \tag{11}$$

For practical considerations, under the assumptions made above regarding the analog and digital beamforming matrices, both equal power allocation per RF chain and equal power distribution across all radiating antenna elements are guaranteed.

To update the digital precoding matrix as the satellite travels in orbit, we propose the event-driven update procedure outlined in Algorithm 1. We introduce the time superscripts (t) and $(t-1)$ to indicate the current and previous time instants, respectively. In this approach, we update the digital precoder only when the analog beamforming matrix $\mathbf{F}_{RF}$ changes due to events such as inter-beam UE handovers, new UEs entering the satellite's service area, or existing UEs exiting the service area. These events occur dynamically and asynchronously, meaning they do not necessarily happen simultaneously or at regular fixed intervals.

TABLE I: Simulation parameters.

Parameter	**Value**
Carrier frequency	20 GHz
Bandwidth	100 MHz
Orbital height	200 - 1200 km
Orbit sampling rate	1000 samples per second
Min. UE elevation angle	30°
$N_x \times N_y$	16×16, 32×32, 45×45
Antenna element spacing	$\lambda/2$
N_{RF}	16
O_x, O_y	2
P_t	15.7 dBW [1]
UE antenna gain	39.7 dBi [1]
UE distribution	Uniform
K	up to 16
Number of UEs per serving beam	1
Simulated satellite pass duration	60 - 420 s
Number of Monte Carlo realizations	250

[1] Values are adopted from [2].

IV. Simulation Results

We conduct Monte Carlo simulations to model the downlink communication between a moving LEO satellite and K stationary UEs. Furthermore, we restrict the number of UEs per beam to one. The simulation parameters are given in Table I.

To gain a comprehensive understanding of the analog beam update rate requirements, which is the time interval after which analog beam realignment is necessary to maintain optimal SNR, we first study the impact of varying orbital altitudes. Based on these findings, we fix the orbital altitude at 600 km to analyze the effect of different antenna array sizes. Finally, we investigate the update rate requirements of the ZF-based digital precoding matrix in terms of its impact on the system sum-rate.

To simplify the scenario, the analysis in Subsections IV-A, IV-B and IV-C assumes that the service area of the satellite is fixed on the ground. Moreover, at the start of the satellite pass, UEs are positioned at the edge of random beams and remain within their respective beams until a better beam in terms of SNR becomes available. This setup represents the

Algorithm 1 Event-driven $\mathbf{F}_{BB}$ update

if $\mathbf{F}_{RF}^{(t)} \neq \mathbf{F}_{RF}^{(t-1)}$ **then**
  for $k = 1 : K$ **do**
    Compute equivalent channel $\hat{\mathbf{h}}_k = \widetilde{\mathbf{h}}_k \, \mathbf{F}_{RF}^{(t)}$.
  end for
  Construct $\hat{\mathbf{H}} = \left[\hat{\mathbf{h}}_1^T, \hat{\mathbf{h}}_2^T, \ldots, \hat{\mathbf{h}}_K^T\right]^T$.
  Compute the ZF precoder $\mathbf{F}_{BB}^{(t)} = \hat{\mathbf{H}}^{\dagger}$.
  Normalize $\mathbf{F}_{BB}^{(t)}$ according to (11).
  Apply the updated precoder $\mathbf{F}_{BB}^{(t)}$
else
  Apply the previous precoder $\mathbf{F}_{BB}^{(t-1)}$.
end if

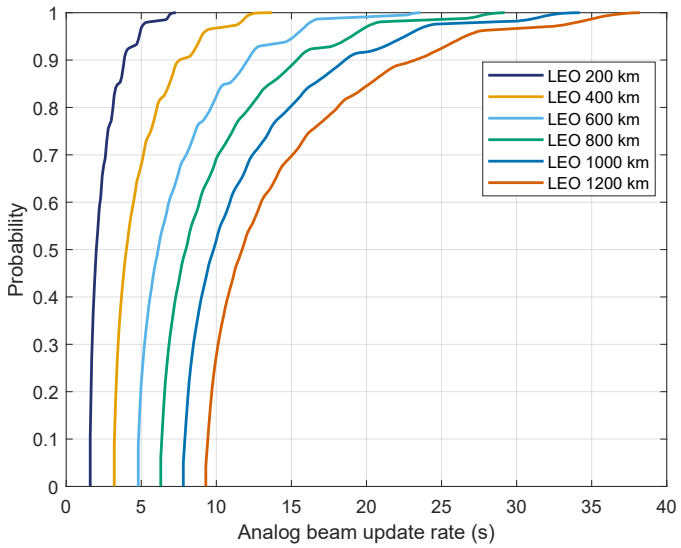

(a) ECDF of beam update rate at various LEO orbital heights.

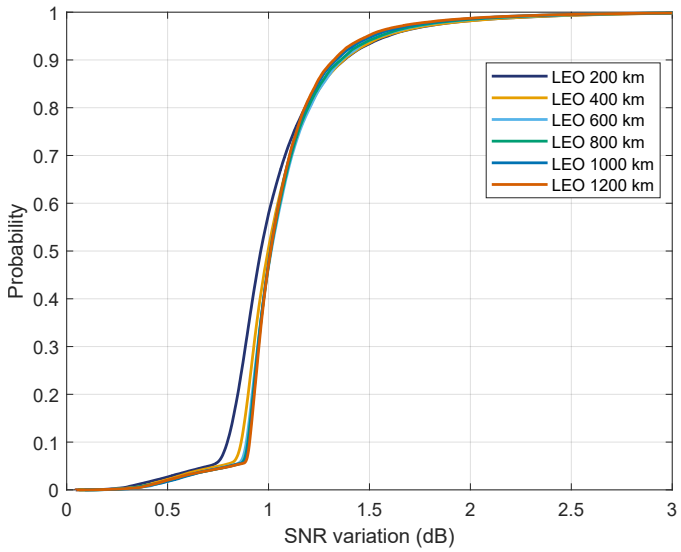

(b) ECDF of UEs SNR variation within their respective beams.

Fig. 2: ECDFs of Analog beam update rate and SNR variation for a 16×16 antenna array at various LEO orbital heights.

maximum possible time a UE spends in a single beam before switching to a better one.

A. Impact of Orbital Height on Analog Beam Update Rate

Fig. 2a shows that lower orbital altitudes necessitate more frequent beam updates. This behavior is attributed to the high relative speed of satellites at lower altitudes and the smaller beam footprint on the ground. In contrast, higher orbital heights exhibit a more gradual increase in the ECDF, as the slower relative motion and larger beam footprint require less updates. Although satellites in lower orbits require more frequent beam updates, the time required for beam realignment is in the order of seconds, which is still manageable at the hardware level. Additionally, more frequent beam updates are necessary for higher elevation angles because the beam footprint is nearly circular at these angles. As the elevation angle decreases, the beam footprint on Earth becomes larger and more elliptical due to the oblique wave incidence on Earth's curvature. The projected 3dB beamwidths of a 16×16 antenna array at Nadir for different LEO orbital heights are given in Table II.

TABLE II: Approximated 3dB beam footprint on Earth for a 16×16 antenna array at Nadir for various LEO altitudes.

Orbital height	**3dB Beam footprint at Nadir**
200 km	23 km
400 km	46 km
600 km	68 km
800 km	92 km
1000 km	114 km
1200 km	136 km

Fig. 2b depicts the SNR variation, defined as the difference between the maximum and minimum SNR within the UEs' serving beam. The results indicate that the SNR variation remains consistent across different orbital altitudes, with the majority of SNR variations clustering around 1 dB. This behavior can be attributed to two factors. First, the UE distribution remains consistent throughout the multi-orbit simulation setup. Second, the beam update strategy, as explained in Subsection III-A, leads to consistent beam transition conditions. To reduce the SNR variation, one may choose to increase the beamforming angular granularity—for example, by oversampling the DFT codebook. However, this also increases inter-beam interference. Conversely, decreasing the beamforming angular granularity by undersampling the DFT codebook increases the SNR variation but also reduces inter-beam interference.

When considering low-complexity LEO satellite systems, pruning the analog beam steering codebooks can significantly reduce beamforming complexity, which is particularly advantageous for large-scale antenna arrays. During the design phase of a satellite mission, a specific service area is typically defined, excluding certain ground stations and UEs from satellite coverage. This service area may have a defined radius or be constrained by a minimum elevation angle. As a result, many codevectors in the codebook become redundant because they correspond to directions outside the defined service area. These redundant codevectors can be pruned using codebook optimization methods, such as the one described in [11]. As illustrated in Fig. 3, our simulation shows that the majority of codevectors in the analog beam steering DFT codebook remain unused. While it is intuitive that codevectors corresponding to directions outside the satellite's service area would remain unused, the unexpectedly high number of unused codevectors is worth noting. This phenomenon is particularly pronounced in satellites, where the beam footprint on the ground expands as the beam's center moves further from the nadir point. Consequently, a reduced number of beams is sufficient to provide effective coverage, rendering many of the codevectors in the codebook redundant. This finding suggests that the codebook can be optimized by eliminating redundant codevectors, potentially reducing computational complexity and hardware requirements. Fig. 4 illustrates this phenomenon by showing an example of a DFT codebook coverage map.

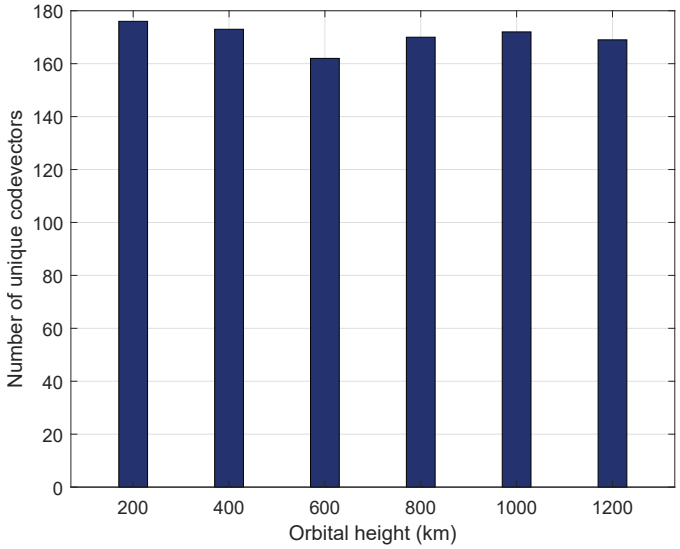

Fig. 3: Number of unique codevectors needed for each simulated LEO orbital height for a 16×16 antenna array.

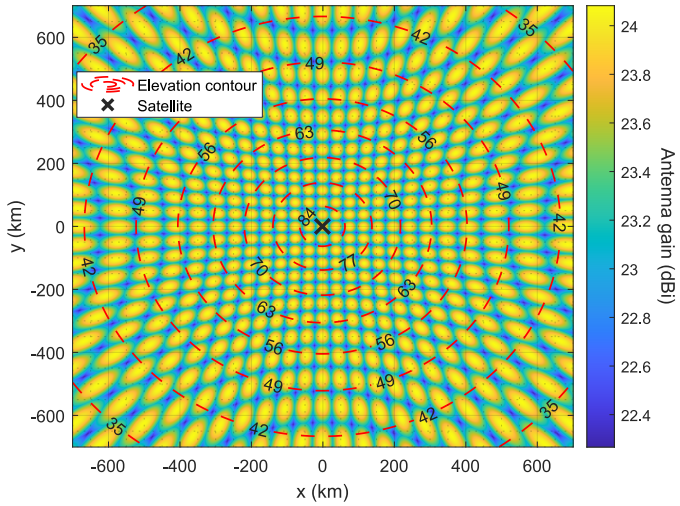

Fig. 4: Best-beam coverage map for a 16×16 antenna array at 600 km LEO. At each point (x, y), we compute the received power from all beams in the DFT codebook and plot the maximum beam power at that location.

Therefore, by disregarding these redundant codevectors, the complexity of the analog beam search can be significantly reduced—in our case, by over 80%.

B. Impact of Antenna Size on Analog Beam Update Rate

The deployment of large antenna arrays in LEO satellites has become a reality, as evidenced by current satellite systems like the AST SpaceMobile's BlueWalker 3 operating in orbit. In [12], the authors conducted a visual count of the number of antenna elements in the BlueWalker 3 satellite image and approximated the number of antenna elements to be around 2368. In light of this, we investigate the performance of antenna arrays of varying dimensions, from the relatively modest 16×16 to the considerably larger 45×45 to assess the analog beam update rate requirements.

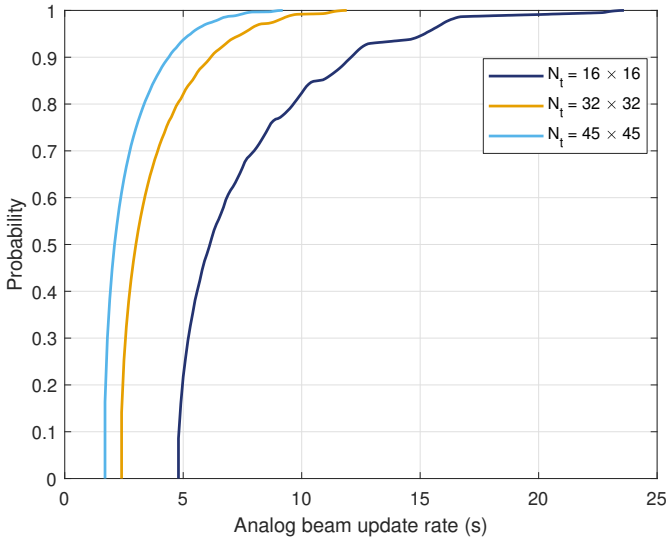

Fig. 5: ECDF of analog beam update rate for various antenna array sizes at 600 km LEO.

TABLE III: Approximated 3dB beam footprint on Earth at Nadir for various antenna array sizes at 600 km LEO.

Antenna Dimensions	**3dB Beam footprint at Nadir**
16×16	68 km
32×32	34 km
45×45	23 km

The analog beam update rate analysis for various antenna array sizes, as depicted in Fig. 5, shows that larger antenna arrays necessitate more frequent beam updates compared to smaller arrays. This is attributed to the decreased beam footprint on the ground as shown in Table III. Specifically, the 45×45 and 32×32 arrays exhibit steep ECDF curves with over 90% of updates occurring within about 5 seconds, reflecting the need for more frequent adjustments to maintain optimal beam alignment. In contrast, the 16×16 array demonstrates more gradual ECDF slopes. This trend indicates that smaller arrays can maintain beam alignment with fewer updates because they produce beams with a wider footprint on the ground. These findings underscore the critical trade-off between antenna array size and analog beam update rate, with larger arrays offering finer angular granularity at the cost of increased computational and operational demands for frequent updates. Our analysis shows that the analog beam update requirements, even for larger arrays with smaller ground footprints, remain manageable in terms of beam switching complexity, typically in the order of seconds.

C. Impact of Digital Precoding Update Rate on Sum-Rate

In this section, we examine the impact of varying update rates of the digital precoding matrix on the system sum-rate. This analysis helps determine the optimal balance between computational complexity and system performance. The results, illustrated in Fig. 6, compare the system sum-rate under various update strategies. To facilitate comparison, we test several

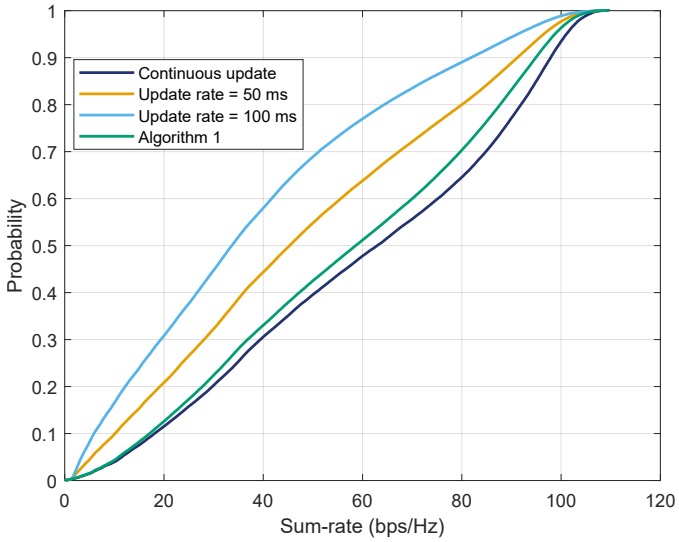

Fig. 6: System sum-rate for different digital precoding matrix update rates for a 16×16 antenna array at 600 km LEO.

different update rates, including: continuous updates—updating the digital precoding matrix at each simulation snapshot, periodic updates—updating every 50 ms and 100 ms, and event-driven updates—updating the digital precoding matrix only when a change occurs in the analog beamforming matrix, as shown in Algorithm 1.

Continuous updating offers the best performance by enabling optimal real-time adaptation to channel state information (CSI). However, it is not feasible in practice because continually updating the digital precoding matrix incurs a high computational cost. Thus, continuous updating represents the upper limit for the system sum-rate of the ZF-based digital precoder and is used as a benchmark for comparison. Since we do not rely on UE feedback in this study, CSI is based on the geometric relation between the satellite and the served UEs as in (8).

Periodic updates of the digital precoding matrix at fixed time intervals show a decline in system performance compared to the benchmark. Although updating every 50 ms approaches the benchmark performance—suggesting that increasing the update frequency offers benefits—it still suffers from CSI aging. Updating at a 100 ms interval results in a further performance decline, as expected, due to the increased effects of CSI aging.

Rather than relying on periodic updates at fixed intervals, we propose the update procedure outlined in Algorithm 1. This mechanism reduces the frequency of digital precoding updates without compromising system performance, maintaining results close to the benchmark as demonstrated in Fig. 6.

It might seem counterintuitive that the procedure in Algorithm 1 can achieve performance comparable to the benchmark, especially when considering Fig.2a, which shows that UEs can remain within the same beam for approximately 5 s or more at 600 km LEO. This discrepancy arises because Fig. 2a illustrates the total duration UEs spend in their respective beams before a transition is required, but it does not indicate when these transitions occur during the simulation. In reality, while some UEs may need to update their beam selection after nearly 5 s from the start of the satellite pass, others will transition much sooner. This results in a staggered distribution of beam transition events among UEs, which is not reflected in Fig.2a.

V. Conclusion

We analyzed beam update rate requirements for LEO satellites using predefined DFT analog beam steering codebooks. Analog beam updates are generally manageable, requiring realignment only every few seconds—even for massive antenna arrays with small Earth footprints. Only a limited subset of codebook beams is utilized during a satellite pass, highlighting the need for codebook optimization in low-complexity LEO missions. Additionally, the ZF-based digital precoder requires frequent updates due to its sensitivity to channel variations and strict interference cancellation requirements. Periodic updates at fixed intervals can degrade system sum-rate because the precoder may not reflect current channel conditions, leading to increased residual interference. While increasing the digital precoder's update frequency improves performance, it raises computational demands. This increased processing may be impractical for low-complexity satellite systems with limited resources. Therefore, implementing an adaptive update strategy is essential to balance performance and computational efficiency.

References

[1] X. Lin, S. Rommer, S. Euler, E. A. Yavuz, and R. S. Karlsson, "5G from space: An overview of 3GPP non-terrestrial networks," *IEEE Communications Standards Magazine*, vol. 5, no. 4, pp. 147–153, 2021.

[2] 3GPP, "3rd Generation Partnership Project; Technical Specification Group Radio Access Network; Solutions for NR to support non-terrestrial networks (NTN) (Release 16)," Tech. Rep. TR 38.821, 3GPP, 2023.

[3] C.-T. Liu and J.-Y. Pan, "Optimal Beamwidth for Maximizing Uplink Coverage Probability in Quasi Earth-Fixed LEO Satellite Communication System," *Electronics*, vol. 13, no. 7, p. 1349, 2024.

[4] M. Caus, A. Perez-Neira, and E. Mendez, "Smart beamforming for direct LEO satellite access of future IoT," *Sensors*, vol. 21, no. 14, p. 4877, 2021.

[5] X. Yu, J.-C. Shen, J. Zhang, and K. B. Letaief, "Alternating minimization algorithms for hybrid precoding in millimeter wave MIMO systems," *IEEE Journal of Selected Topics in Signal Processing*, vol. 10, no. 3, pp. 485–500, 2016.

[6] J. Zhang, X. Yu, and K. B. Letaief, "Hybrid beamforming for 5G and beyond millimeter-wave systems: A holistic view," *IEEE Open Journal of the Communications Society*, vol. 1, pp. 77–91, 2019.

[7] S. Mabrouki, I. Dayoub, Q. Li, and M. Berbineau, "Codebook designs for millimeter-wave communication systems in both low-and high-mobility: Achievements and challenges," *IEEE access : practical innovations, open solutions*, vol. 10, pp. 25786–25810, 2022.

[8] M. Choi and W. Sung, "A Next-Generation Codebook Evolution Strategy for Massive Arrays Using Deep Neurals Networks," *International Journal of Antennas and Propagation*, vol. 2022, no. 1, p. 3837376, 2022.

[9] M. Momani and M. Nabeel, "Towards Realistic Stochastic Channel Modeling for Mobility-Enabled Low Earth Orbit Satellites," in *2023 IEEE Conference on Standards for Communications and Networking (CSCN)*, pp. 159–164, IEEE, 2023.

[10] A. Alkhateeb, G. Leus, and R. W. Heath, "Limited feedback hybrid precoding for multi-user millimeter wave systems," *IEEE transactions on wireless communications*, vol. 14, no. 11, pp. 6481–6494, 2015.

[11] J. Palacios, N. González-Prelcic, C. Mosquera, T. Shimizu, and C.-H. Wang, "A hybrid beamforming design for massive MIMO LEO satellite communications," *Frontiers in Space Technologies*, vol. 2, p. 696464, 2021.

[12] D. Tuzi, T. Delamotte, and A. Knopp, "Satellite swarm-based antenna arrays for 6G direct-to-cell connectivity," *IEEE Access*, vol. 11, pp. 36907–36928, 2023.